Check for updates

Preparation of magnetic urchin-like NiCo$_2$O$_4$ powders by hydrothermal synthesis for catalytic oxidative desulfurization

Qinlin Yuan,[a] Fengmin Wu, [ID] [a] Hang Xu, [ID] *[ab] Xiaowei Wang,[a] Jie Luo,[a] Yakun Song,[a] Yafei Guo[a] and Xuefeng Wei[ab]

In this manuscript, magnetic NiCo$_2$O$_4$ powder was prepared by hydrothermal synthesis and utilized as a catalyst to remove dibenzothiophene (DBT) from *n*-octane. The results showed that the average particle size, Langmuir surface area, and average pore diameter of synthetic NiCo$_2$O$_4$ powders were 15 nm, 998.7 m^2 g^{-1}, and 19.6 nm, respectively. The magnetic urchin-like NiCo$_2$O$_4$ powder formed by linear directional agglomeration of rectangular NiCo$_2$O$_4$ nano-flakes followed by agglomeration of NiCo$_2$O$_4$ nano-wires, and subsequently urchin-like agglomeration of NiCo$_2$O$_4$ bundles. The NiCo$_2$O$_4$ powder exhibited excellent magnetic separation ability, recycling stability, and catalytic activity. The NiCo$_2$O$_4$ powder activated peroxymonosulfate (PMS) to produce a highly reactive oxygen species for oxidizing DBT to DBT-sulfoxide. The sulfur removal was ~98% under the following optimum conditions: 6 mL of model oil (600 ppm), PMS with oxygen to the sulfur ratio of 3 : 1, 0.5 g of NiCo$_2$O$_4$ powder, 40 °C, and 20 min. Interestingly, the NiCo$_2$O$_4$ catalyst maintained high activity after being reused five times.

1. Introduction

The past couple of decades have witnessed a significant development of industrialization. In contrast, an increase in fossil fuels such as gasoline, diesel, and kerosene consumption and demand has been correspondingly accompanied by an increase in the emission of hazardous sulfur oxides (SO$_x$).[1] At the same time, organic sulfur compounds in fuels (*e.g.*, sulfides, disulfides, and thiophene) were converted to SO$_x$ during combustion, creating severe environmental concerns such as smog and acid rain, which caused respiratory problems and threatening our health.[2,3] In recent years, stringent environmental legislation on fuel limited the sulfur content to the ultralow ppm levels (<10 ppm), posing great challenges to refiners together.[4,5] The surging environmental crisis has stimulated the unprecedented demand for clean, efficient, and economic desulfurization technologies.

Hydro-desulfurization (HDS), a mature well-studied process, has been proven to be effective for sulfur removal down to 500 ppm for fuel feedstock.[6] Nevertheless, HDS requires demanding conditions from strong pressures (20–100 atm), high temperatures (>300 °C) to expensive catalysts, leading to increased capital and operating costs.[7] Besides, HDS is difficult

to get down to 15 or 10 ppm for deep desulfurization.[8,9] Therefore, researchers have been searching for a lot of alternative ways to remove sulfur compounds, including extractive desulfurization, adsorptive desulfurization, oxidative desulfurization (ODS), biological desulfurization, alkylation-based, chlorinolysis-based, and supercritical water-based desulfurization.[10–12]

ODS is one of the most advanced and promising methods of removing sulfur compounds from fuel through the oxidation reaction with mild reaction conditions and low investment.[13,14] In a recent study, Wang *et al.* showed that the total efficiency of desulfurization from thiophene with ozone near 100% could be obtained with the SO$_4^{2-}$/ZrO$_2$ catalytic oxidation reaction.[15] Guo *et al.* showed excellent desulfurization performance under relatively mild conditions by using ODS.[16] Generally, the ODS process involves two stages, including oxidation/sulfone generation and separation.[17,18] The immediate goal of high sulfur removal can be achieved with ODS. However, scientists are still searching for catalysts and oxidants to remove sulfur compounds effortlessly and efficiently under mild conditions.[19] Over the years, a variety of oxidants such as H$_2$O$_2$, molecular oxygen, organic peracids, and *tert*-butyl hydroperoxide (TBHP) have been reported in the literature.[20–23] Peroxymonosulfate (PMS) has received increasing attention because of its strong oxidizing ability.[24,25] Sulfate radicals possess high redox potential (2.5–3.1 V)[26] based on the activation methods. Additionally, it shows higher selectivity and longer half-life compared to other radicals in certain cases. In addition, a solid powder does not easily decompose and loses efficiency, which exhibits

[a]School of Chemical Engineering and Pharmacy, Henan University of Science and Technology, Luoyang, 471023, China. E-mail: xhinbj@126.com

[b]Provincial and Ministerial Co-Construction of Collaborative Innovation Center for Non-Ferrous Metal New Materials and Advanced Processing Technology, Luoyang 471023, China

certain advantages concerning transportation, storage, and use compared to a liquid oxidizer.[27] This strong, stable, cheap, and environmentally friendly oxidizing agent can be activated by microwave heat and many other ways.[28–30] In particular, cobalt compounds are widely used to activate PMS owing to their excellent catalytic activities.[31] Therefore, sulfate radicals could be expected to show excellent capacity in ODS.

Nickel cobaltite ($NiCo_2O_4$) is an interesting mixed-valence composite transition metal oxide with a spinel structure. $NiCo_2O_4$ has gained much interest in several applications, including electrocatalytic, photocatalytic, supercapacitors, microwave-assisted Fenton reaction, and oil/water separation, due to its broad light absorption range, multiple states of transition metal elements, excellent chemical stability, and low leaching of heavy metals.[32–35] Additionally, the synergistic effect between the Ni and Co components results in a significant enhancement in catalytic activity compared with the corresponding single individual oxides (NiO and Co_3O_4). This exhibits richer redox properties (both Ni^{2+} and Co^{3+} are active species), much higher electronic conductivity, higher catalytic activity, lower cost and most importantly environmentally benign in nature.[36,37] These benefits enable $NiCo_2O_4$ to be a promising candidate as a catalyst. In the last few years, PMS activated by $NiCo_2O_4$ has been extensively studied. A recent report suggested the employment of $NiCo_2O_4$ for the degradation of sulfamethoxazole in model wastewater by activation of PMS.[38] Tian *et al.* have reported PMS oxidation over $NiCo_2O_4$ provided a promising alternative for humic acid degradation due to its efficient catalytic activity.[39] Zhang *et al.* have reported that $NiCo_2O_4$ catalyst completely degrades Rhodamine B (RhB) dye within 30 min with the assistance of PMS.[34] Di *et al.* prepared $NiCo_2O_4$ nanoarrays and used them as high-efficiency electrodes to activate PMS to bleach RhB with high efficiency.[40] To date, there were few efforts have been devoted to $NiCo_2O_4$ powders as a heterogeneous catalyst by PMS activation in removing sulfur compounds from oil.

In this study, magnetic $NiCo_2O_4$ powder was prepared by the hydrothermal method and utilized as the catalyst to activate PMS for removing dibenzothiophene (DBT), a sulfur-containing organism, from *n*-octane. The micro-structure of the $NiCo_2O_4$ catalyst was analyzed by XRD, TEM, SEM, BET and VSM. The product after desulfurization was analyzed by GC-MS and the desulfurization mechanism was also discussed.

2. Experimental

2.1 Preparation of $NiCo_2O_4$ powders

Cobalt chloride ($CoCl_2 \cdot 6H_2O$, 1.1897 g), nickel chloride ($NiCl_2 \cdot 6H_2O$, 0.5942 g), hexadecyl trimethyl ammonium bromide (CTAB, 0.9109 g) and urea (CH_4N_2O, 1.35 g) were dissolved in deionized water (37.5 mL). After stirring 30 min in 25 °C, the transparent solution was transferred to a 100 mL Teflon-lined autoclave. The hydrothermal process was conducted at 160 °C for 6 h. The precipitate was collected by vacuum filtration, washed several times, and then dried in a vacuum oven at 70 °C for 6 h. Finally, the dried precipitate was calcined at 350 °C for 3 h to obtain $NiCo_2O_4$ powder.[41–43]

2.2 Desulfurization process

The simulated oil with 600 ppm initial sulfur content was prepared by dissolving dibenzothiophene (DBT) in *n*-octane. 100 mg $NiCo_2O_4$ was added to 10 mL of simulated oil and acetonitrile, and stirred vigorously for 30 min to achieve adsorption and extraction equilibrium. When 0.5 mL PMS (20 wt%) solution (O/S = 3 : 1) was added to acetonitrile, the catalytic oxidative desulfurization process was started. After 10 min, the desulfurization reaction was finished and the supernatant was detected by UV-visible spectrophotometer (Shimadzu UV-2700). After desulfurization, the catalyst was magnetically separated, washed, and dried.

2.3 General information & characterization

All the chemical reagents were purchased from Sigma-Aldrich Shanghai Company. The specific surface area and pore size distribution of $NiCo_2O_4$ powder were tested by BET analyzer (Quantachrome NOVA400). The magnetic property of $NiCo_2O_4$ powder was measured by vibrating sample magnetometer (LakeShore7404). The surface morphology and microstructure were studied by scanning electron microscopy (GeminiSEM 300) and transmission electron microscopy (FEI Tecnai G2 F20). The product, after desulfurization, was analyzed by gas chromatography mass spectrometry (Trace GC Ultra-ISQ, Thermo Fisher).

3. Results and discussion

3.1 Characterizations of $NiCo_2O_4$ powder

As-synthesized $NiCo_2O_4$ was characterized using several spectroscopic and microscopic studies. The powder X-ray diffraction pattern of the as-synthesized $NiCo_2O_4$ powder showed the characteristic peaks of 2θ which are located at 18.90°, 31.15°, 36.70°, 38.40°, 44.62°, 55.43°, 59.09°, 64.98° and 77.54° corresponded to (111), (220), (311), (222), (400), (422), (511), (440) and (533) plane of cubic $NiCo_2O_4$, respectively (Fig. 1(a)).[42] The XRD pattern is consistent with the JCPDS 20-0781 standard card. No distinct impurity peak was detected, indicating that the pure $NiCo_2O_4$ powders were obtained by hydrothermal method.

Magnetic measurement was performed to understand the magnetic behavior of $NiCo_2O_4$. The typical magnetic hysteresis loops of $NiCo_2O_4$ powder with the magnetic field of ±4000 Oe were observed (Fig. 1(b)). The magnetic saturation (MS) value of the $NiCo_2O_4$ powder was found to be 6 emu g^{-1}. VSM measurement also demonstrated the typical magnetic behavior of $NiCo_2O_4$. The presence of magnetic property indicates that $NiCo_2O_4$ can be efficiently and conveniently separated from the simulated oil by an external magnet.

Next, the porous nature of $NiCo_2O_4$ was determined by the N_2 adsorption study. The N_2 adsorption–desorption curves, as shown in Fig. 1(c), are closer to the X-axis in the low-pressure area (0–0.1) and the medium-pressure area (0.3–0.8), which implied that the N_2 adsorption force on material surface is modest. The curves are more inclined to the *y*-axis in the high-pressure area (0.8–1.0), indicating a significant rise in N_2 self-adsorption capacity. Moreover, the absorption–desorption
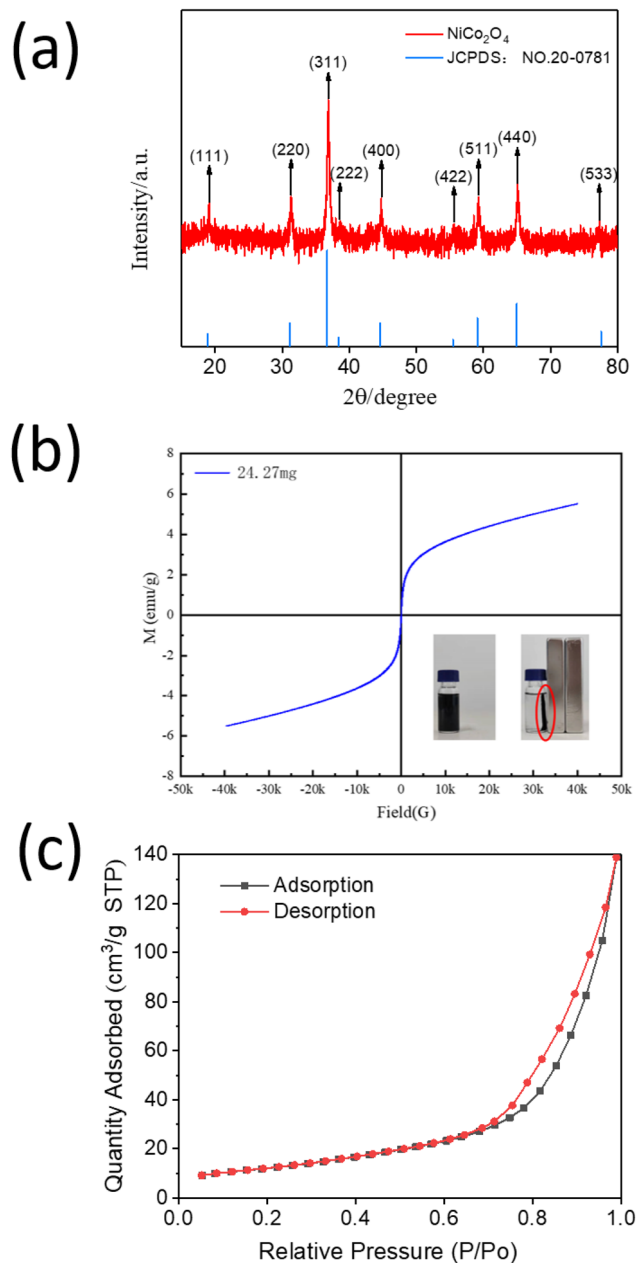
Fig. 1 Characterization of $NiCo_2O_4$ powders ((a) XRD; (b) VSM; (c) N_2-adsorption desorption).

curves exhibit a typical hysteresis loop attributable to the type IV isotherm according to the IUPAC classification, which is a noteworthy property of mesoporous material. According to the hysteresis loop categorization of IUPAC, the $NiCo_2O_4$ powder displayed a typical H3 type feature, demonstrating the mesoporous structure of $NiCo_2O_4$ which was generated between the slits of flake particles.

3.2 The mechanism of $NiCo_2O_4$ formation

The microscopy study unveiled the formation mechanism of $NiCo_2O_4$. Fig. 2(a–c) shows the morphology images of the $NiCo_2O_4$ powder as observed by transmission electron

microscopy (TEM) at different magnifications and selected area electron diffraction (SAED) patterns. As shown in Fig. 2(a), the urchin-like morphology of $NiCo_2O_4$ powders was observed with ~5 μm of particle size. Fig. 2(b) illustrates the linear accumulation of nano-$NiCo_2O_4$ particles to form nanowires that look like urchin stings. These urchin stings can improve the catalytic sites and thus lead to the rise of catalytic activity. HRTEM image displayed the nano-$NiCo_2O_4$ particles are rectangular thin flakes with ~15 nm average particle size. Meanwhile, the SAED pattern is in good agreement with standard data ICSD 00-020-0781 (Fig. 2(c)). The diffraction rings are attributable to the (311), (400), (440), and (444) planes. Additionally, the HRTEM image elucidated the lattice spacing of $NiCo_2O_4$ nano-particle showing distinct lattice planes and implying good crystallinity of the prepared $NiCo_2O_4$. In addition, the d-spacing is 0.2463 nm, which is by the (311) planes of $NiCo_2O_4$ (JCPDS 20-0781). The SEM image of the $NiCo_2O_4$ powder is shown in Fig. 2(d). SEM image demonstrated the rough micro-surface of $NiCo_2O_4$ powders which are stacked as a bundle of one-dimensional nanowires.

Based on the HRTEM and SEM study, the mechanism of urchin-like $NiCo_2O_4$ formation is demonstrated in Fig. 2(e). The formation pathway involved linear directional agglomeration of nano-$NiCo_2O_4$ particles followed by binding agglomeration of $NiCo_2O_4$ wires, which is consistent with Zhang's study.[44] Ultimately, the $NiCo_2O_4$ bundle was agglomerated to form urchin-like particles, more and more nanowires self-assembled together and the urchin-like microsphere is formed consequently, which is consistent with Zhang's research.[45]

3.3 Catalytic oxidative desulfurization of $NiCo_2O_4$ powder

Acetonitrile has low surface tension and facilitates easy mass transfer at the biphasic solvent interface. What is more, acetonitrile, with a better extraction effect on dibenzothiophene, is selected as an extractor as a typical solvent, leading to a higher desulfurization rate. The produced $DBTO_2$ can be extracted from model oil by acetonitrile solvent, which significantly enhanced the ODS efficiency of $NiCo_2O_4$ in this work.[46] Therefore, by using acetonitrile as an extractant, it is significant for us to investigate the catalytic performance of the $NiCo_2O_4$ in the extractive catalytic oxidative desulfurization (ECODS) experiments.

From −30 min to 0 min, there was only a simple extraction desulfurization process, while no oxidation desulfurization process. From −30 min to 0 min was a process of extraction gradually reaching equilibrium. The oxidant was applied at 0 min (extraction equilibrium), and only then did it start the real extraction oxidation desulfurization reaction.

The effect of $NiCo_2O_4$ powder dosage on sulfur removal was evaluated (Fig. 3(a)). The desulfurization efficiencies of $NiCo_2O_4$ dosages increased with $NiCo_2O_4$ powder dosages varied from 20 mg to 80 mg within 20 min. The result indicated that more active sites were generated for the activation of PMS. The sulfur removal efficiency reached up to 98% within only 20 min with a catalyst loading of 80 mg. However, the desulfurization effect remained intact with 100 mg of loading. The mesoporous
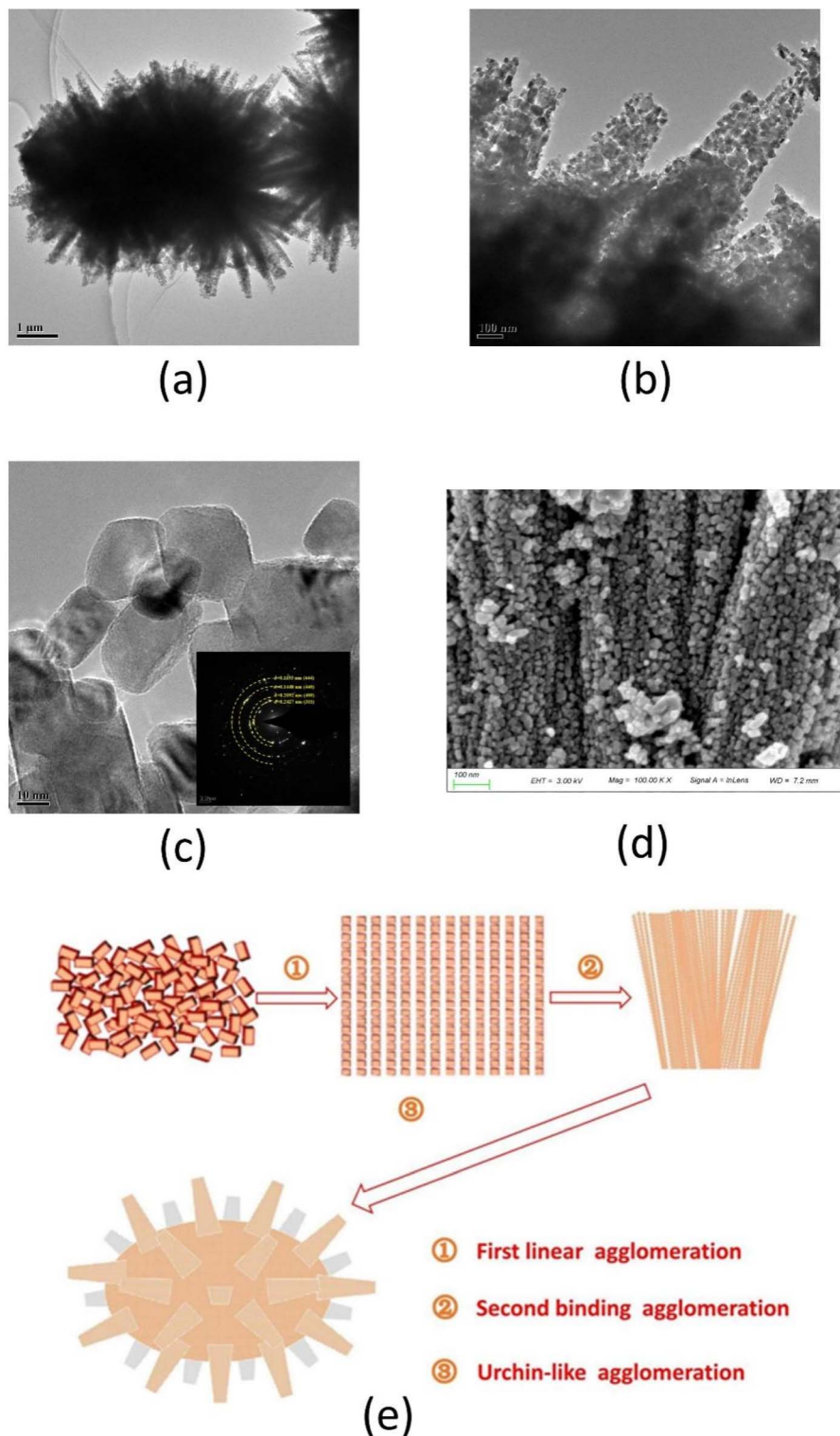
Fig. 2 The forming mechanism of NiCo$_2$O$_4$ powders ((a) TEM image; (b) partial enlarged drawing of image (a); (c) HRTEM and SAED pattern; (d) SEM image; (e) agglomeration mechanism image).

nature of NiCo$_2$O$_4$ assisted the diffusion of the substrate. The relatively large channel was more suitable for the adsorption and desorption of large sulfur-containing substances compared to the narrow channeled materials. Moreover, it also indicated that the NiCo$_2$O$_4$ and PMS combined system possessed excellent desulfurization rates.

Fig. 3(b) demonstrated the desulfurization rates at different desulfurization temperatures. In the extraction stage, DBT was
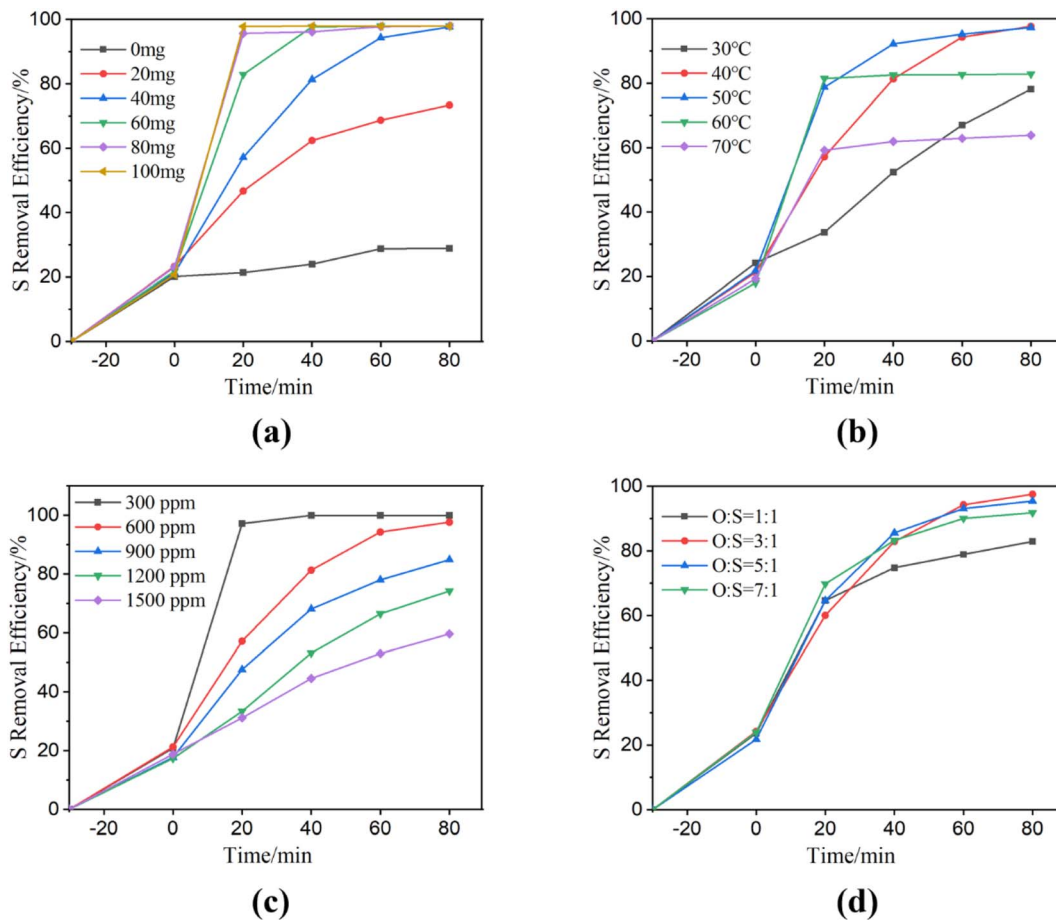
Fig. 3 Catalytic oxidative desulfurization of NiCo$_2$O$_4$ powders at different experimental conditions ((a) NiCo$_2$O$_4$ dosage; (b) temperature; (c) DBT initial dosage; (d) O : S ratio).

diffused from the oil phase to the extraction phase. As shown in Fig. 3(b), desulfurization rates are 24.19%, 21.23%, 21.69%, 18.00% and 19.31% at extraction temperatures of 30, 40, 50, 60 and 70 °C, respectively. After the addition of PMS into the system, the desulfurization rate was improved with the increase in temperatures. The sulfur removal efficiencies significantly increased in the range from 30 °C to 50 °C within 60 min. However, the desulfurization rate decreased when the temperature increased to 60 °C or 70 °C. The exorbitant high temperature is not favorable for catalytic oxidation.[47] In addition, PMS is not stable and decomposes easily at 65 °C.[48] The desulfurization rate increased with the increase of temperature in the first 60 min, but at 80 min, the desulfurization rate at 40 °C was as high as that at 50 °C, reaching the desulfurization rate up to 97.65%. Regarding economic considerations and taking into account the time required for almost complete removal of DBT, the temperature of 40 °C is considered as optimal temperature.

Fig. 3(c) showed the effect of the initial DBT concentration on the desulfurization process. The increase in the initial sulfur contents from 300 to 1500 ppm led to a decrease in the removal efficiencies from 21.2 to 17.3% in the first extraction region. In the second extraction–oxidation catalytic desulfurization (EOCDS) region, the sulfur removal efficiencies significantly

increased within the first 20 min for all the initial sulfur content concentrations. NiCo$_2$O$_4$ can catalyze PMS to produce a large number of HSO$_5^-$ due to its excellent catalytic activity, so its desulfurization efficiency is significantly and rapidly improved. The sulfur removal efficiencies at 80 min were 99.98%, 97.65%, 84.89%, 74.25%, and 59.64% for the initial sulfur contents of 300, 600, 900, 1200, and 1500 ppm, respectively. At constant initial NiCo$_2$O$_4$ dosage and PMS dosage, the sulfur removal efficiency decreased when the concentration of the target substance was high enough. The sulfur removal efficiency decreased with the rise of initial sulfur content.

A suitable oxygen to sulfur ratio (O/S), using the correct amount of PMS (20 wt%), is crucial to obtaining an efficient ODS process. If the O/S ratio is too low, the ability of the system to oxidize DBT in the model oil will be compromised.[49] However, excess PMS is not favorable for the catalytic oxidation ability of cobalt ions. Therefore, a suitable PMS dosage is important. Fig. 3(d) demonstrated the desulfurization rate increased from 82.90% to 97.54%, with the O/S ratio increasing from 1 : 1 to 3 : 1. Furthermore, when the O/S ratios further increased from 3 : 1 to 7 : 1, the desulfurization rate decreased slightly. The experimental results may be attributed to the content of PMS exceeding the optimum value because the

RSC Advances Paper

Table 1 Comparative analysis of DBT removal efficiency *via* ODS from reported literature and present study

Catalyst	Oxidant	Dosage (g L^{-1})	Concentration (ppm)	O/S ratio	Temperature (°C)	Time (min)	S removal efficiency (%)	Ref.
NiCo$_2$O$_4$	PMS	13	600	3	40	20	98	Present study
CoMoO HNCs-0.3	O$_2$	0.2	500	—	110	60	100	51
CoMo/rGO	H$_2$O$_2$	6.4	500	30	60	60	99	52
Fe–Ni–Mo/Al$_2$O$_3$	H$_2$O$_2$	40	800	15.8	60	150	99	53
Co/KIT-6	CYHPO	8	400	5.7	93	40	98.68	54
[Co$_3$(oba)$_3$(O) (Py) 0.5]$_n$·4DMF·Py	TBHP	4	500	3	60	480	75.2	55
CoW/rGO	H$_2$O$_2$	7.2	500	6	60	45	100	56

strong acidity from hydrogen persulfate is not favorable for the catalytic oxidation of cobalt ions. Moreover, hydrogen persulfate also serves as the scavenger of sulfate radical,[50] which is not favorable for the reaction. Therefore, the optimal O/S ratio for the desulfurization system is found to be 3 : 1.

As shown in Table 1, compared with other cobalt-containing or nickel-containing catalysts, the NiCo$_2$O$_4$ catalyst has the shortest reaction time, the lowest required temperature and the lowest amount of oxidant under the same efficiency.[51–56]
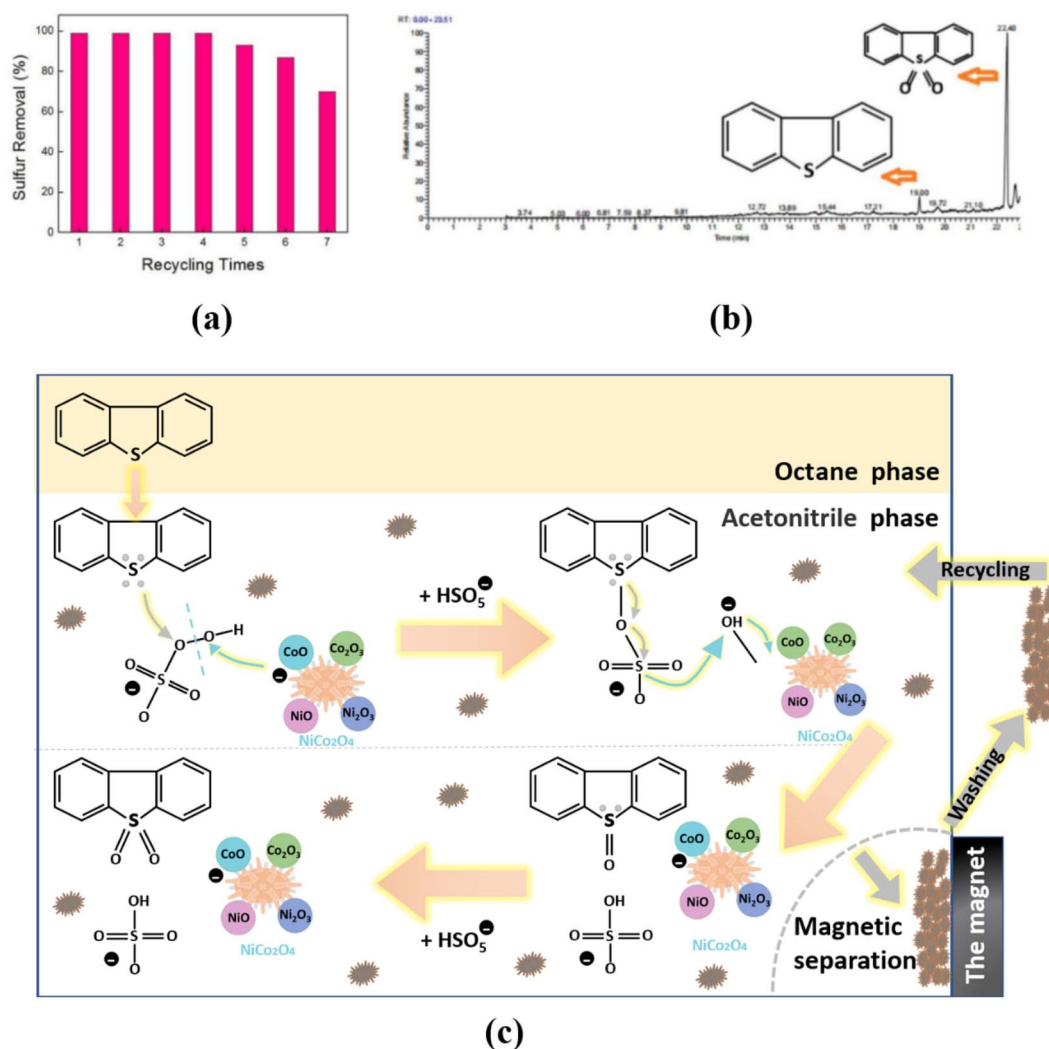

Fig. 4 Catalytic oxidative desulfurization of NiCo$_2$O$_4$ powders ((a) recycling test; (b) GC-MS analysis of oxidative product; (c) possible desulfurization mechanism).

3.4 Recycling of NiCo₂O₄ powder and desulfurization mechanism

Recycling ability was verified for $NiCo_2O_4$ catalyst which maintained a good desulfurization effect with ~99% sulfur removal after being used four times (Fig. 4(a)). However, after fifth cycle of desulfurization test, the desulfurization rate was 87%, and the activity of the catalyst decreased by ~12%. The deactivation of the catalyst could be caused by the contamination of the active sites of the catalyst and the destruction of the catalyst structure after repeated use. Fig. 4(b) displays the GC-MS analysis of simulated oil after the desulfurization process, and the oxidative product was DBT-sulfoxide ($DBTO_2$).

Therefore, a possible desulfurization mechanism was constructed and shown in Fig. 4(c). Firstly, according to the similarity-intermiscibility theory,[57] nonpolar DBT is readily soluble in nonpolar octane, at which point DBT only has an extraction process. At the extraction equilibrium, only about 20% DBT was extracted by acetonitrile at most.

When the PMS was added to the reaction system, DBT is oxidized to a polar $DBTO/DBTO_2$ product, it can be successfully extracted by acetonitrile as a polar solvent and separated from the oil phase. Thusly, the higher polar $DBTO_2$ was kept in the extractant phase, which resulted in a continuous reduction in DBT concentration in the oil phase. So $NiCo_2O_4$ can effectively enhance the ODS efficiency of DBT. In the acetonitrile phase, the possible specific oxidation reaction mechanism is as follows.

In the acetonitrile phase, the CoO can catalyze the cleavage of the peroxide bridge of HSO_5^- to produce sulfate radicals (SO_4^-) and hydroxyl radicals. Meanwhile, CoO can give one of its electrons to the hydroxyl radical and form an unstable Co–O covalent bond. The sulfate radical can attack lone pair electrons of sulfur atom in DBT molecule. The electron cloud density of sulfur is relatively high, which is conducive to the formation of covalent double bonds with an oxygen atom. Therefore, DBT can be oxidized to form DBTO. The unstable Co–O covalent bond can obtain an electron from the S–O bond in HSO_5^- to form a stable CoO. Briefly, the HSO_5^- can release the active oxygen to form S=O bond under $NiCo_2O_4$ as a catalyst. $DBTO_2$ can also be produced in a similar mechanism.

After the reaction, the interaction of $NiCo_2O_4$ with $DBTO_2$ is reduced because the electron-bonding ability of S atoms in $DBTO_2$ is severely decreased. Therefore, the oxidation product ($DBTO_2$) can be desorbed and released from the surface of the catalyst. In addition, the $DBTO_2$ can thoroughly dissolve in acetonitrile because the polarity of its S=O bonds is considerably stronger than the polarity of the S–C bonds in DBT using electronegativity analysis.[58]

4. Conclusion

In summary, magnetic urchin-like $NiCo_2O_4$ powder was prepared by hydrothermal technology. The microstructure of obtained $NiCo_2O_4$ and the formation mechanism of nanomaterials are speculated. The Langmuir surface area and average pore diameter of $NiCo_2O_4$ were 998.7 m² g⁻¹ and

19.6 nm, respectively. The $NiCo_2O_4$ powder exhibited excellent magnetic separation ability, recycling stability, and catalytic oxidation capability to activate PMS for removing DBT from *n*-octane. The sulfur removal was ~98% under the optimized condition. The reaction system exhibited excellent dibenzothiophene (DBT,4,6-DMDBT) removal under the optimum experimental conditions. The $NiCo_2O_4$ catalyst maintained high activity after being reused five times. Therefore, $NiCo_2O_4$ catalysts possess great potential for application in oxidative desulfurization. Finally, the possible desulfurization mechanism was also discussed.

Conflicts of interest

The authors declare that they have no known competing financial interests or personal relationships that could have appeared to influence the work reported in this paper.

Acknowledgements

References

1 M. Hayyan, M. H. Ibrahim, A. Hayyan, I. M. AlNashef, A. M. Alakrach and M. A. Hashim, *Ind. Eng. Chem. Res.*, 2015, **54**, 12263–12269.

2 A. Hassan, S. Z. Ilyas, A. Jalil and Z. Ullah, *Environ. Sci. Pollut. Res.*, 2021, **28**, 21204–21211.

3 D. V. Wagle, H. Zhao, C. A. Deakyne and G. A. Baker, *ACS Sustainable Chem. Eng.*, 2018, **6**, 7525–7531.

4 H. Xu, D. Zhang, F. Wu and R. Cao, *Fuel*, 2017, **208**, 508–513.

5 L. Hao, M. J. Hurlock, X. Li, G. Ding, K. W. Kriegsman, X. Guo and Q. Zhang, *Catal. Today*, 2020, **350**, 64–70.

6 J.-W. Ding and R. Wang, *Chin. Chem. Lett.*, 2016, **27**, 655–658.

7 V. Chandra Srivastava, *RSC Adv.*, 2012, **2**, 759–783.

8 H. Shang, W. Du, Z. Liu and H. Zhang, *J. Ind. Eng. Chem.*, 2013, **19**, 1061–1068.

9 X. Chen, H. Guo, A. A. Abdeltawab, Y. Guan, S. S. Al-Deyab, G. Yu and L. Yu, *Energy Fuels*, 2015, **29**, 2998–3003.

10 B. Rodríguez-Cabo, H. Rodríguez, E. Rodil, A. Arce and A. Soto, *Fuel*, 2014, **117**, 882–889.

11 B. Jiang, H. Yang, L. Zhang, R. Zhang, Y. Sun and Y. Huang, *Chem. Eng. J.*, 2016, **283**, 89–96.

12 N. Gupta, P. K. Roychoudhury and J. K. Deb, *Appl. Microbiol. Biotechnol.*, 2005, **66**, 356–366.

13 T.-C. Chen, Y.-H. Shen, W.-J. Lee, C.-C. Lin and M.-W. Wan, *J. Cleaner Prod.*, 2013, **39**, 129–136.

14 J. Li, Z. Yang, S. Li, Q. Jin and J. Zhao, *J. Ind. Eng. Chem.*, 2020, **82**, 1–16.

15 B. Wang, J. Zhu and H. Ma, *J. Hazard. Mater.*, 2009, **164**, 256–264.

16 Y.-F. Guo, C.-Y. Gao, K.-G. Yang, Z.-J. Wang, Y.-H. Duan, S.-X. Feng and H. Xu, *Energy Fuels*, 2019, **33**, 10728–10733.

17 M. H. Ibrahim, M. Hayyan, M. A. Hashim and A. Hayyan, *Renewable Sustainable Energy Rev.*, 2017, **76**, 1534–1549.

18 Z. Wu and B. Ondruschka, *Ultrason. Sonochem.*, 2010, **17**, 1027–1032.

19 M. Haghighi and S. Gooneh-Farahani, *Environ. Sci. Pollut. Res.*, 2020, **27**, 39923–39945.

20 F. S. Mjalli, O. U. Ahmed, T. Al-Wahaibi, Y. Al-Wahaibi and I. M. AlNashef, *Rev. Chem. Eng.*, 2014, **30**, 337–378.

21 C. Gong, F. Chen, Q. Yang, K. Luo, F. Yao, S. Wang, X. Wang, J. Wu, X. Li, D. Wang and G. Zeng, *Chem. Eng. J.*, 2017, **321**, 222–232.

22 A. Wang, Z. Chen, Z. Zheng, H. Xu, H. Wang, K. Hu and K. Yan, *Chem. Eng. J.*, 2020, **379**, 122340.

23 H. Zhang, Q. Ji, L. Lai, G. Yao and B. Lai, *Chin. Chem. Lett.*, 2019, **30**, 1129–1132.

24 J. Miao, Y. Zhu, J. Lang, J. Zhang, S. Cheng, B. Zhou, L. Zhang, P. J. J. Alvarez and M. Long, *ACS Catal.*, 2021, **11**, 9569–9577.

25 W. Wang, Y. Liu, Y. Yue, H. Wang, G. Cheng, C. Gao, C. Chen, Y. Ai, Z. Chen and X. Wang, *ACS Catal.*, 2021, **11**, 11256–11265.

26 C. Liang, C. F. Huang and Y. J. Chen, *Water Res.*, 2008, **42**, 4091–4100.

27 H. Xu, J. Zhang, D. Zhang, Y. Guo and F. Wu, *Fuel*, 2021, **288**, 119655.

28 Y. Qi, Q. Zuo, Y. Mei, T. Yao and J. Wu, *ACS Appl. Nano Mater.*, 2020, **3**, 7152–7160.

29 J. Hu, X. Zeng, G. Wang, B. Qian, Y. Liu, X. Hu, B. He, L. Zhang and X. Zhang, *Chem. Eng. J.*, 2020, **400**, 125869.

30 Y. Liu, Y. Wang, Q. Wang, J. Pan and J. Zhang, *Chemosphere*, 2018, **190**, 431–441.

31 Y.-Y. Ahn, H. Bae, H.-I. Kim, S.-H. Kim, J.-H. Kim, S.-G. Lee and J. Lee, *Appl. Catal., B*, 2019, **241**, 561–569.

32 H. Chen and J. Wang, *Chemosphere*, 2021, **268**, 128840.

33 S. Zhang, Y. Xu, J. Tu, M. Li, L. Zhi, D. Hu and J. Liu, *J. Mater. Sci.*, 2021, **56**, 6645–6662.

34 W. Zhang, Y. Su, X. Zhang, Y. Yang and X. Guo, *RSC Adv.*, 2016, **6**, 64626–64633.

35 T. Kim, A. Ramadoss, B. Saravanakumar, G. K. Veerasubramani and S. J. Kim, *Appl. Surf. Sci.*, 2016, **370**, 452–458.

36 M. Silambarasan, P. S. Ramesh and D. Geetha, *J. Mater. Sci.: Mater. Electron.*, 2016, **28**, 323–336.

37 J. Du, G. Zhou, H. Zhang, C. Cheng, J. Ma, W. Wei, L. Chen and T. Wang, *ACS Appl. Mater. Interfaces*, 2013, **5**, 7405–7409.

38 M. Xu, H. Zhou, Z. Wu, N. Li, Z. Xiong, G. Yao and B. Lai, *J. Hazard. Mater.*, 2020, **399**, 123103.

39 X. Tian, C. Tian, Y. Nie, C. Dai, C. Yang, N. Tian, Z. Zhou, Y. Li and Y. Wang, *Chem. Eng. J.*, 2018, **331**, 144–151.

40 J. Di, M. Zhu, R. Jamakanga, X. Gai, Y. Li and R. Yang, *J. Water Process. Eng.*, 2020, **37**, 2214–7144.

41 Z.-Q. Liu, K. Xiao, Q.-Z. Xu, N. Li, Y.-Z. Su, H.-J. Wang and S. Chen, *RSC Adv.*, 2013, **3**, 4372–4380.

42 Y. Li, X. Wu, S. Wang, W. Wang, Y. Xiang, C. Dai, Z. Liu, Z. He and X. Wu, *RSC Adv.*, 2017, **7**, 36909–36916.

43 S. x. Yan, S. h. Luo, M. z. Sun, Q. Wang, Y. h. Zhang and X. Liu, *Int. J. Energy Res.*, 2021, **45**, 20186–20198.

44 S. Zhang, H. Gao, J. Zhou, F. Jiang and Z. Zhang, *J. Alloys Compd.*, 2019, **792**, 474–480.

45 X. Q. Zhang, Y. C. Zhao, C. G. Wang, X. Li, J. D. Liu, G. H. Yue and Z. D. Zhou, *J. Mater. Sci.*, 2016, **51**, 9296–9305.

46 M. Dadashi, G. Mazloom, A. Akbari and F. Banisharif, *Environ. Sci. Pollut. Res. Int.*, 2020, **27**(24), 30600–30614.

47 H. Li, W. Zhu, Y. Wang, J. Zhang, J. Lu and Y. Yan, *Green Chem.*, 2009, **11**, 810–815.

48 A. M. Kermani, A. Ahmadpour, T. R. Bastami and M. Ghahramaninezhad, *New J. Chem.*, 2018, **42**, 12188–12197.

49 C. Zhang, X. Pan, F. Wang and X. Liu, *Fuel*, 2012, **102**, 580–584.

50 J. Madhavan, P. Maruthamuthu, S. Murugesan and S. Anandan, *Appl. Catal., B*, 2008, **83**, 8–14.

51 J. Guo, L. Chu, L. Wang, H. Liu, M. Yang and G. Wang, *Appl. Surf. Sci.*, 2022, **579**, 0169–4332.

52 S. Hasannia, M. Kazemeini, A. Rashidi and A. Seif, *Appl. Surf. Sci.*, 2020, **527**, 146798.

53 Y. Muhammad, A. Shoukat, A. U. Rahman, H. U. Rashid and W. Ahmad, *Chin. J. Chem. Eng.*, 2018, **26**, 593–600.

54 S. Wei, H. He, Y. Cheng, C. Yang, G. Zeng, L. Kang, H. Qian and C. Zhu, *Fuel*, 2017, **200**, 11–21.

55 M. Y. Masoomi, M. Bagheri and A. Morsali, *Inorg. Chem.*, 2015, **54**, 11269–11275.

56 S. Hasannia, M. Kazemeini, A. Seif and A. Rashidi, *Sep. Purif. Technol.*, 2021, **269**, 1383–5866.

57 J. Wang, W. Wu, H. Ye, Y. Zhao, W.-H. Wang and M. Bao, *RSC Adv.*, 2017, **7**, 44827–44833.

58 M. A. Rezvani and N. Khalafi, *Mater. Today Commun.*, 2020, **22**, 100730.